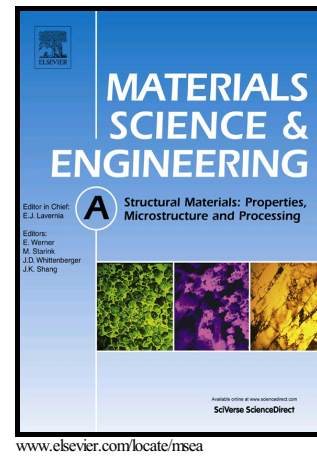


Author's Accepted Manuscript

Strengthening of A2024 alloy by high-pressure torsion and subsequent aging

Intan Fadhlina Mohamed, Takahiro Masuda, Seungwon Lee, Kaveh Edalati, Zenji Horita, Shoichi Hirosawa, Kenji Matsuda, Daisuke Terada, Mohd Zaidi Omar



PII: S0921-5093(17)30988-7
DOI: <http://dx.doi.org/10.1016/j.msea.2017.07.083>
Reference: MSA35331

To appear in: *Materials Science & Engineering A*

Received date: 21 March 2017
Revised date: 25 July 2017
Accepted date: 26 July 2017

Cite this article as: Intan Fadhlina Mohamed, Takahiro Masuda, Seungwon Lee, Kaveh Edalati, Zenji Horita, Shoichi Hirosawa, Kenji Matsuda, Daisuke Terada, and Mohd Zaidi Omar, Strengthening of A2024 alloy by high-pressure torsion and subsequent aging, *Materials Science & Engineering A* <http://dx.doi.org/10.1016/j.msea.2017.07.083>

This is a PDF file of an unedited manuscript that has been accepted for publication. As a service to our customers we are providing this early version of the manuscript. The manuscript will undergo copyediting, typesetting, and review of the resulting galley proof before it is published in its final citable form. Please note that during the production process errors may be discovered which could affect the content, and all legal disclaimers that apply to the journal pertain.

Strengthening of A2024 alloy by high-pressure torsion and subsequent aging

Intan Fadhlina Mohamed^{1,2,3}, Takahiro Masuda^{1,2}, Seungwon Lee^{1,2,4},
Kaveh Edalati^{1,2}, Zenji Horita^{1,2}, Shoichi Hirosawa⁵, Kenji Matsuda⁴,
Daisuke Terada⁶ and Mohd Zaidi Omar³

¹Department of Materials Science and Engineering, Faculty of Engineering, Kyushu University, Fukuoka 819-0395, Japan

²WPI, International Institute for Carbon-Neutral Energy Research (I²CNER), Kyushu University, Fukuoka 819-0395, Japan

³Department of Mechanical and Materials Engineering, Faculty of Engineering and Built Environment, Universiti Kebangsaan Malaysia, 43600 UKM Bangi, Selangor, Malaysia

⁴Graduate School of Science and Engineering for Research, University of Toyama, Toyama 930-8555, Japan

⁵Department of Mechanical Engineering and Materials Science, Yokohama National University, Yokohama 240-8501, Japan

⁶Department of Mechanical Science and Engineering, Faculty of Engineering, Chiba Institute of Technology, Narashino 275-0016, Japan

An age-hardenable A2024 alloy is processed by high-pressure torsion (HPT) for grain refinement and further aged for fine precipitation. The HPT is conducted under an applied pressure of 6 GPa for 0.75, 1 and 5 turns with a rotation speed of 1 rpm at room temperature and this results in a significant grain size reduction to a grain size of ~240±80 nm. The hardness sharply increases with imposing strain at an early stage but

level off after 5 turns. Further aging at temperatures of 373 K and 423 K leads to extra hardening above the elevated hardness of the HPT-processed condition. Components contributing to the strengthening were evaluated in terms of grain refinement and fine precipitation including the contributions from dislocation accumulation and solid solution. In this study, a conclusion is reached such that simultaneous strengthening due to grain refinement and fine precipitation is achieved by application of HPT processing and subsequent aging.

*Corresponding author: Intan Fadhlina Mohamed

Tel/Fax: +603-89216864; E-mail: intanfadhlina@ukm.edu.my

1. Introduction

Grain refinement is a useful means for strengthening of metallic materials as predicted from the Hall-Petch relation [1,2]. It is confirmed that significant grain refinement is attained in bulk metallic materials irrespective of sample states when they are processed by techniques of severe plastic deformation (SPD) [3,4]. Several SPD processing techniques are available [4] but the most promising appears to be high-pressure torsion (HPT) because this process produces an ultrafine-grained microstructure with high-angle boundaries [5]. Evaluating closely some past research reports [6-9], the HPT process is more effective in grain refinement than other SPD processes as equal-channel angular pressing (ECAP). It was also shown that, when additional straining is imposed by HPT on ECAP-processed pure Ti with a grain size of ~300 nm, further refinement of the grain size to ~200 nm is achieved [10].

Besides the grain refinement, fine dispersion of precipitate particles through aging treatment is also effective to enhance the strength of metallic materials as it may be expected from the Orowan theory [11]. It was reported that age hardenable aluminum 2xxx alloys is strengthened by solute cluster as fast as 60 s [12]. The most probable precipitation phases was shown in earlier findings [13].

Although the SPD process has been reported widely due to the high potential to refine grain size and thus lead to significant increase in strength, reports are rather limited for the simultaneous increase in strength due to grain refinement and fine dispersion of particles. Recently, Hirosawa *et al.* proposed three strategies to effectively achieve the simultaneous strengthening [14], and some successful results were reported on the Al-Mg-Si system [14-19], Al-Ag system [20, 21], Al-Li-Cu-Mg system [22] and Al-Zn-Mg-Cu system [23, 24]. Some reports are also available for the Al-Cu system from the study by Kim *et al.* [25] and the recent study by the authors' group [26-28].

However, for the former study by Kim *et al.* [25], the grain refinement with high-angle boundaries was not sufficiently attained because ECAP process was feasible only for 1 pass without breaking. The investigation by the authors' group was carried out using HPT process but mainly undertaken in the Al-Cu binary system without impurity elements, which thus led to grain coarsening during aging treatment after the HPT processing [27]. We reported a preliminary result on an A2024 alloy which is the Al-Cu system with commercial purity that the strengthening is achieved by the HPT processing and subsequent aging [26]. However, no quantitative evaluation was attempted for the strengthening mechanism. Thus, the current research is initiated to conduct in a more comprehensive way: first to cover the conditions for HPT processing and aging for optimization of the strengthening, and second to clarify the mechanism for the strengthening. The quantitative evaluation for the strengthening includes not only the contribution from grain refinement and fine precipitation but also from other effects such as dislocation accumulation and solid solution hardening.

2. Experimental procedures

This study used a commercial A2024 alloy (4.6% Cu, 1.5% Mg, 0.6% Mn, 0.24% Fe, 0.09% Si, 0.07% Zn, 0.03% Cr, 0.01% Ti and 0.01% Ti+Zr with balance of Al in wt%). An as-received rod with 10mm diameter was sliced into discs with 1mm thickness using a wire-cutting electrical discharge machine (EDM). The discs were subjected to solution treatment at 793 K for 12 h and then immediately quenched in ice water. HPT processing was conducted at room temperature (R.T.) for three different turns (N) as $N = 0.75, 1$ and 5 under an applied pressure of 6 GPa with a rotation speed of 1 rpm. The initial thickness of 1 mm was reduced to 0.8-0.85 mm by the HPT processing. The HPT-processed discs were aged at 373 K and 423 K for up to 10 days to

evaluate the thermal stability and aging behavior.

The discs were ground by sand papers and polished to a mirror-like surface. The Vickers microhardness was measured by applying 100 g for duration of 15 s using a Mitutoyo HM-102 tester. The hardness measurements were made along 8 radial directions where each indentation was done at equal distance from the disc center toward the edge as shown in Fig. 1.

Fig.1 also depicts the dimensions of tensile specimens and the positions where tensile specimens were extracted. The gauge part of the tensile specimen is 2 mm away from the disc center.

For transmission electron microscopy (TEM), discs with 3mm diameter were extracted from the center part of the HPT-processed disk as shown in Fig. 1 and were thinned to perforation using a twin-jet electro-polisher in a solution of 25% HNO_3 and 75% $\text{C}_2\text{H}_5\text{OH}$ at a temperature of 263 K under an applied voltage of 15 V. All TEM specimens were analysed by a Hitachi H-8100 transmission electron microscope at an accelerating voltage of 200 kV. Average grain sizes were determined from dark-field images by measuring at least 100 different grains with well-defined boundaries. Selected area electron diffraction (SAED) patterns were taken from a region with 6.3 μm diameter.

The 3mm discs with 0.4mm thickness were prepared for XRD analysis using the Cu $K\alpha$ radiation with an accelerating voltage of 40 kV and a current of 40 mA. The $K\alpha_2$ radiation was filtered out from the XRD profile to avoid the influence. The dislocation densities were measured from peak broadening using the Williamson-Hall method [29]

3. Results

3.1 Mechanical properties and microstructure evolutions with HPT processing

Figure 2 (a) plots the Vickers microhardness against the distance from the disc center after $N = 0.75, 1$ and 5 turns. The hardness after HPT processing significantly increases above the dotted lines of the solution-treated samples. However, the hardness variation with respect to the distance from the disc centre is different depending on the numbers of turns. The hardness increase is more notable after 5 turns than 0.75 and 1 turns. The hardness saturation occurs at a position closer to the disc center after 5 turns but it is shifted to the edges of the discs after 0.75 and 1 turns.

All hardness values in Fig. 2 (a) are plotted as a function of the equivalent strain in Fig. 2 (b) as attempted in earlier papers [30-32], which is calculated from the following equation:

$$\varepsilon = 2\pi Nr / \sqrt{3}h \quad (1)$$

Here, ε is the equivalent strain, N is the number of revolution, r is the distance from the disc center and h is the thickness of the disc after HPT processing. As in Fig. 2 (b), the hardness change is well described by a particular function of the equivalent strain. The hardness increases drastically at the early stage of straining and starts to saturate when the equivalent strain comes to ~ 20 . Further increasing in straining led to a uniform hardness state where the hardness remain constant at level of ~ 250 Hv. Despite the fact that the equivalent strain is zero at the disc center according to eq.(1), close inspection of Fig. 2 (a) reveals that the hardness at the disc center increases with increasing N . In practice, hardness measurement at the real center is difficult but the hardness values were measured within the radial circle of 0.2 mm around the center. Furthermore, a little misalignment of the rotation axes between the lower and upper anvils during HPT

process may cause introduction of an extra shear strain near the center of the disc even the alignment was adjusted well within ± 0.01 mm in this experiment.

The results of tensile testing are shown in Fig. 3 for $N = 0.75, 1$ and 5 turns including solution treated states. The tensile strength increases with the number of turns and reaches the tensile strength of 910 MPa with the elongation to failure about 5% . Fig. 4 shows the summary of tensile strength and elongation to failure with respect to the numbers of turns. The tensile strength increases sharply with HPT straining and the elongation to failure decreases but still maintains the elongation to failure more than 5% . This tensile strength is higher by ~ 200 MPa than the one reported by Kim *et al.* in the same A2024 alloy [25] and by 100 MPa than our earlier report in an Al-4%Cu binary alloy [27]. It is well demonstrated that the high strength is achieved with reasonable ductility by the HPT processing.

Figure 5 shows a series of bright-field images (left) and dark-field images (right) and the corresponding SAED patterns (center) after HPT processing of the samples at three different states taken from samples subjected to different magnitudes of equivalent strains: (a) $\varepsilon \approx 1$ after processing for 0.75 turns, (b) $\varepsilon \approx 16$ after processing for 1 turn and (c) $\varepsilon \approx 80$ after processing for 5 turns. The arrows in the SAED patterns mark the selected diffraction beams for the corresponding dark-field images. At the early stage of straining, a high density of entangled dislocations is observed within the grains as shown in the dark-field images in Fig. 5(a). With straining to $\varepsilon \approx 16$, fewer dislocations are visible and the grain boundaries are straight and more defined as in Fig. 5(b). As the hardness increases to the saturated level, the grain size becomes smaller and the SAED pattern exhibits a ring-like form as in Fig. 5(c). The evolution of the SAED pattern from a web-like in Fig. 5(a) to a ring-like in Fig. 5(c) indicates an increase in the misorientation angles between neighbouring grains.

Based on the variation of hardness in Fig. 2 and the microstructural evolution in Fig. 5, the grain refinement of this alloy may be achieved in the way similar to earlier observations [5, 31]. Many dislocations were generated as anticipated from the normal deformation mode and thus the dislocations coalesce to form subgrains. Consequently, pronounced strain hardening takes place due to an increase in the stored strain energy through dislocations accumulation. With further straining, the subgrain size decreases with simultaneous increase in the dislocation density within the subgrains. The subgrain boundaries become better defined and the misorientation angle increases.

The distribution of the grain size is shown in Fig.6 from the microstructures after 5 tuns, where 100 grains were measured in dark-field images as shown in Fig.5(c). The measurement led to an average grain size of ~240 nm but it turned out that the microstructure consists of grains with sizes in a wide range as ~90 nm to ~410 nm.

3.2 Effect of aging

When aging was undertaken at 373 K and 423 K, an appreciable increase in hardness is realized above the as-HPT-processed level as shown in Fig. 7(a). The peak hardness reaches earlier when aged at the higher temperature: 30 min at 423 K and 4 h at 373 K. Figure 7(b) plots the amount of the hardness increase above the as-HPT-processed level.

Microstructures including SAED patterns are shown in Fig. 8 for the steady state conditions after aging at 423 K for (a) 30 min and (b) 4 h. All micrographs were taken at the saturated level of hardness. There appears to be no appreciable difference in the images after the two different aging times, but with prolonged aging for 4 h, superlattice spots are visible in the SAED pattern as marked by red lines in Fig. 8(b), indicating the formation of S-phase (Al_2CuMg) precipitates.

Figure 9 shows the variations of grain size and dislocation density with the aging time along with the variation of the hardness for the samples processed by HPT through 5 turns and subsequently aged at 423 K. No appreciable grain growth occurs during the peak aging (30 min) and overaging (4h): $\sim 260 \pm 80$ nm and $\sim 260 \pm 90$ nm, respectively. However, the dislocation density decreases due to recovery (annihilation) during the aging. Nevertheless, the aging behaviour of the hardness exhibits the opposite trend until the peak age, and thus this indicates that the contribution from the precipitation hardening well exceeds the softening due to dislocation annihilation.

4. Discussion

4.1 Strengthening components

In order to quantify the increase in hardness during aging, a schematic model is depicted in Fig.10 where the total strength can be represented by an additive law of strengthening components such as solid solution hardening, grain boundary hardening, dislocation hardening and precipitation hardening. Based on the current study, there are no changes in the grain size through the aging. However, the dislocation density diminishes during the aging. Nevertheless, the hardness increases during the aging to the peak value and then decreases when the aging is prolonged. Thus, the increase in hardness at the beginning of aging is neither due to the increase in the grain size nor the decrease in the dislocation density but this can be explained by the hardening due to precipitation.

4.1.1 Solid solution hardening

Solid solution hardening may occur in the A2024 alloy because the alloy contains elements such as Cu and Mg partly in a form of solid solution. Such elements

differ from the matrix atoms in size and/or in shear modulus to cause variation and distortion of strain field. It has been widely used that solid-solution hardening is estimated by the Fleishcher equation [33] or Labusch equation [34] as given in the following forms, respectively.

$$\Delta\tau_{ss} = \frac{G|\varepsilon'_G - m\varepsilon_b|^{3/2} c^{1/2}}{\alpha} \quad (2)$$

$$\Delta\tau_{ss} = \frac{G[\varepsilon'^2_G + (15\varepsilon_b)^2]^{2/3} c^{2/3}}{\varphi} \quad (3)$$

The meaning and values of G , ε'_G , ε_b , m , φ and α are given in Table 1 [35]. Since the solute concentration, c of the minor alloying elements such as Fe, Si, Zn, Cr, Ti, Tl and Zr are small (within $<0.0001 - 0.0011$), the contributions from these elements are ignored. Therefore, the calculation of the solid solution hardening was considered only from the primary alloying elements, Cu where $c = 0.0190$ and Mg where $c = 0.0162$. Here, the estimation yields $\Delta\tau_{ss} = 4.8$ MPa and $\Delta\tau_{ss} = 0.1$ MPa for Cu and Mg by the Fleischer equations, and $\Delta\tau_{ss} = 8.2$ MPa and $\Delta\tau_{ss} = 5.8$ MPa by applying Labusch equations, respectively. The calculation by both Fleischer and Labusch finally yields the contribution of $HV = 4.4$ Hv and 7.5 Hv in Cu and $HV = 0.1$ Hv and 5.3 Hv in Mg, where the relationship ΔHV (Hv: kg/mm^2) = $0.9\Delta\tau$ (MPa) was used to convert the shear stress to the Vickers hardness. It follows that both primary solute elements, Cu and Mg, have minor contribution in this alloy.

4.1.2 Grain boundary hardening

The most significant consequence of the HPT processing is the grain refinement may disrupt dislocation movement through introducing new high volume density of grain boundaries so as retarding the dislocation from propagate to the

adjacent grains, thereby strengthening the materials. The most significant consequence of the HPT processing is the grain refinement so that the dislocation movement is blocked by a high volumetric density of grain boundaries and the propagation to the adjacent grains is difficult, thereby strengthening the materials. The grain boundary strengthening mechanism is usually described by the Hall-Petch relation [1, 2] as follows.

$$\Delta\sigma_{GB} = \sigma_y - \sigma_0 = \frac{k_y}{\sqrt{d}} \quad (4)$$

The Hall-Petch coefficient, k_y [36] is given in Table 1. For the present study, therefore, the increase in yield strength due to grain boundary hardening is calculated to be 265 MPa which is converted to 81 Hv.

4.1.3 Dislocation hardening

The contribution by dislocation accumulation to the strengthening may be estimated by the following Bailey-Hirsch equation [36].

$$\Delta\tau_{Dis} = \alpha' Gb\sqrt{\rho} \quad (5)$$

Here, ρ is the dislocation density and the values of G , b and α' are given in Table 1. For the as-HPT-processed state, the value of ρ was obtained as $\sim 8.9 \times 10^{14} \text{ m}^{-2}$. However, it was reduced to $\sim 7.0 \times 10^{14} \text{ m}^{-2}$ after aging for 30 min at 423 K (peak age) and to $\sim 5.7 \times 10^{14} \text{ m}^{-2}$ when the aging was prolonged to 4 h (overage). Thus, the strength contributed by dislocation hardening are determined as 41 Hv, 36 Hv and 33 Hv in the as-HPT-processed state and the states after 30min aging (peak age) and 4h aging (overage), respectively.

4.1.4 Precipitation hardening

Estimation of the precipitation hardening may be given by the Orowan theory through the following equation [11].

$$\Delta\tau_p = \frac{Gb}{\lambda'} \quad (6)$$

The values of G and b are given in Table 1 and λ' is the inter-particle spacing defined as $\lambda' = L - d_p$ where d_p is the particle size and L is the distance between particles. In this study, the dispersion of precipitates was not well detected because the particles might have been too small or few to be observed in the as-HPT-processed samples after aging for 30 min although the aging result shows the increase in hardness. However, the precipitates were visible after prolonged aging for 4 h. In estimating the strengthening due to precipitation for the peak aging, earlier study showed that even the presence of a few precipitates in an ultrafine grain are sufficient to account for the increase in the strength [20]. Provided that two precipitates with an average size of 30 nm are present in a grain with an average grain size of 260 nm, the distance between adjacent precipitates and grain boundaries becomes $\lambda' = 70$ nm. This finally yields the contribution of $\Delta\tau_{ss} = 106$ MPa, and thus the conversion to hardness leads to 95 Hv.

4.2 Quantitative evaluation for total strengthening

All components contributing to the strengthening are summarized in Table 2. The dominant contributions are from grain boundary strengthening (ΔHV_{GB}) and precipitate strengthening (ΔHV_p). A moderate contribution is from dislocations strengthening (ΔHV_{Dis}) but the minor contribution from solid solution hardening (ΔHV_{ss}). From this information, it should be possible to estimate the total strength of the as-HPT-processed sample and the sample processed by HPT with additional

precipitation hardening. The contributions from the different strengthening factors are added linearly so that the total strength of the A2024 alloy, HV_{Total} , is given as [37].

$$\Delta HV_{Total} = HV_0 + \Delta HV_{SS} + \Delta HV_{GB} + \Delta HV_{Dis} + \Delta HV_P \quad (7)$$

Here, HV_0 was taken as 20 Hv based on direct measurement of the lattice friction stress for pure Al [39]. This value can be acceptable because the lattice parameter for the matrix of the alloys obtained from the X-ray diffraction is in agreement with the value for pure Al within experimental errors. Using the result in Table 2, HV_{Total} shows reasonable agreement with the measured values but, nevertheless, the lower estimation may result from an underestimation for the precipitates strengthening which is based on the assumption that 2 precipitates are located in the grain interiors while, in a real conditions, there might be more precipitates. Most recently, Chen *et al* observed the formation of clusters in atomic levels, which might be responsible for the underestimation [40].

In this alloy, it was observed that the hardening by aging is followed by softening but the softening rate is slower when the aging temperature is reduced. In particular, the alloy maintains their hardness levels higher than those of the as-HPT-processed conditions even after prolonged aging as shown in Fig. 7. Meanwhile, the dislocation density decreases through the aging and the grain size remains unchanged with aging at 373 K and 423 K. Thus, it is worthwhile addressing that the increase in the hardness during the initial stage of aging was neither due to the grain growth nor the dislocation recovery but it is due to hardening by precipitation. It is well demonstrated that the A2024 alloy exhibits concurrent strengthening due to grain refinement by HPT processing and fine precipitation by subsequent aging.

5. Summary and Conclusions

1. Significant grain refinement occurs in 0.75, 1 and 5 turns up to size of $\sim 240 \pm 80$ nm and the hardness increased by 2.5 times due to HPT processing.
2. The hardness increases rapidly at the beginning of straining and saturates to a constant level of 250 Hv at higher straining.
3. The tensile strength at the saturated level reaches 910 MPa with the total elongation to fracture of $\sim 5\%$.
4. Grain refinement and precipitation of fine particles is attained and lead to concurrent strengthening when the sample processed by HPT for 5 turns are aged at 373 K and 423 K.
5. Two hardening components due to grain refinement and fine precipitation contribute significantly to the total strengthening, while dislocation hardening is moderate and solid solution hardening is minor.

Acknowledgments

IFM thanks Universiti Kebangsaan Malaysia (the National University of Malaysia) for awarding Young Researcher Encouragement Grant (GGPM-2016-029) and the Ministry of Higher Education Malaysia for the Fundamental Research Grant Scheme (FRGS/1/2016/TK03/UKM/02/4). IFM also gratefully acknowledges SIRIM Berhad Company of Malaysian Government for a scholarship. This work was supported in part by Japan Science and Technology Agency (JST) under Collaborative Research Based on Industrial Demand “Heterogeneous Structure Control: Towards Innovative Development of Metallic Structural Materials”, in part by the Light Metals Educational Foundation of Japan, and in part by a Grant-in-Aid for Scientific Research (S) from the MEXT, Japan (No.26220909). The HPT process was carried out in the International

Research Center on Giant Straining for Advanced Materials (IRC-GSAM) at Kyushu
University

Accepted manuscript

References

- [1] E.O. Hall, The deformation and aging of mild steel III, *Proc. Phys. Soc. B*, 64 (1951) 747-753.
- [2] N.J. Petch, The cleavage strength of polycrystals, *J. Iron Steel Inst.* 174 (1953) 25-28.
- [3] R.Z. Valiev, R.K. Islamgaliev, Alexandrov IV, Bulk nanostructures materials from severe plastic deformation, *Prog. Mater. Sci.* (2000) 103-189.
- [4] R.Z. Valiev, Y. Estrin, Z. Horita, T.G. Langdon, M.J. Zehetbauer, Y.T. Zhu, Producing bulk ultrafine-grained materials by severe plastic deformation, *JOM* 58(4) (2006) 33-39.
- [5] Y. Ito, Z. Horita, Microstructural evolution in pure aluminum processed by high-pressure torsion, *Mater. Sci. Eng. A*, 503, (2009) 32-36.
- [6] Y. Iwahashi, Z. Horita, M. Nemoto, T.G. Langdon, Factors influencing the equilibrium grain size in equal-channel angular pressing: role of Mg additions to aluminum, *Metall. Mater. Trans. A* 29 (1998) 2503-2510.
- [7] Z. Horita, D.J. Smith, M. Furukawa, M. Nemoto M, R.Z. Valiev, T.G. Langdon, An Investigation of Grain Boundaries in Submicrometer-Grained Al-Mg Solid Solution Alloys Using High-Resolution Electron Microscopy, *J. Mater. Res.* 11 (1996) 1880-1890.
- [8] A.P. Zhilyaev, S. Lee, G.V. Nurislamova, R.Z. Valiev, T.G. Langdon, Microhardness and microstructural evolution in pure nickel during high-pressure torsion, *Scr. Mater.* 44 (2001) 2753-2758.
- [9] A.P. Zhilyaev, B.K. Kim, G.V. Nurislamova, M.D. Baro, J.A. Szpunar, T.G. Langdon, Orientation imaging microscopy of ultrafine-grained nickel, *Scr. Mater.* 48 (2002) 575-580.
- [10] V.V. Stolyarov, Y.T. Zhu, T.C. Lowe, R.K. Islamgaliev, R.Z. Valiev, A two steps SPD processing of ultrafine-grained titanium, *Nanostruct. Mater.* 11 (1999) 947-954.
- [11] E. Orowan, Discussion on internal stresses. Symposium on Internal Stresses in Metals and Alloys, The Institute of Metal, London, (1948) 451-453.
- [12] S.P. Ringer, T. Sakurai, I.J. Polmear, Origins of hardening in aged Al-Cu-Mg-Ag alloys, *Acta Mater.* 45 (1997) 3731-3744.
- [13] S.P. Ringer, I.J. Polmear, T. Sakurai, Effect of additions of Si and Ag to ternary Al-Cu-Mg-Ag alloys in the $\alpha + S$ phase field, *Mater. Sci. Eng. A* 217 (1996) 273-276.
- [14] S. Hirosawa, T. Hamaoka, Z. Horita, S. Lee, K. Matsuda, D. Terada, Methods for designing concurrently strengthened severely deformed age-hardenable aluminum

alloys by ultrafine-grained and precipitation hardenings, *Metall. Mater. Trans. A* 44A (2013) 2013-3921.

[15] W.J. Kim, J.K. Kim, T.J. Park, S.I. Hong, D.I. Kim, Y.S. Kim, J.D. Lee, Enhancement of strength and superplasticity in a 6061 Al alloy processed by equal-channel-angular-pressing, *Metall. Mater. Trans. A* 33 (2002) 3155-3164.

[16] J.K. Kim, H.K. Kim, J.W. Park, W.J. Kim, Large enhancement in mechanical properties of the 6061 Al alloys after a single pressing by ECAP, *Scr. Mater.* 53 (2005) 1207-1211.

[17] D. Akama, S. Lee, Z. Horita, K. Matsuda, S. Hirosawa, Aging behavior of ultrafine-grained Al-Mg-Si-X (X=Cu, Ag, Pt, Pd) alloys produced by high-pressure torsion, *Mater. Trans.* 55 (2014) 640-645.

[18] I.F. Mohamed, S. Lee, K. Edalati, Z. Horita, S. Hirosawa, K. Matsuda, D. Terada, Aging behavior of Al 6061 alloy processed by high-pressure torsion and subsequent aging, *Metall. Mater. Trans. A* 46 (2015) 2664-2673.

[19] X. Sauvage, S. Lee, K. Matsuda, Z. Horita, Origin of the influence of Cu or Ag micro-additions on the age hardening behavior of ultrafine-grained Al-Mg-Si alloys, *J. Alloys Compd.* 710 (2017) 199-204.

[20] Z. Horita, K. Ohashi, T. Fujita, K. Kaneko, T.G. Langdon, Achieving high strength and high ductility in precipitation-hardened alloys, *Adv. Mater.* 17 (2005) 1599-1602.

[21] K. Ohashi, T. Fujita, K. Kaneko, Z. Horita and T.G. Langdon, The aging characteristics of an Al-Ag alloy processed by equal-channel angular pressing, *Mater. Sci. Eng., A* 437 (2006) 240-247.

[22] S. Lee, Z. Horita, S. Hirosawa, K. Matsuda, Age-hardening of an Al-Li-Cu-Mg alloy (2091) processed by high-pressure torsion, *Mater. Sci. Eng. A* 546 (2012) 82-89.

[23] S. Lee, K. Tazoe, I.F. Mohamed, Z. Horita, Strengthening of AA7075 alloy by processing with high-pressure sliding (HPS) and subsequent aging, *Mater. Sci. Eng. A* 628 (2015) 56-61.

[24] Y.H. Zhao, X.Z. Liao, S. Cheng, E. Ma, Y.T. Zhu, Simultaneously increasing the ductility and strength of nanostructured alloys, *Adv. Mater.* 18 (2006) 2280-2283.

[25] W.J. Kim, C.S. Chung, D.S. Ma, S.I. Hong, H.K. Kim, Optimization of strength and ductility of 2024 Al by equal channel angular pressing (ECAP) and post-ECAP aging, *Scr. Mater.* 49 (2003) 333-338.

[26] I.F. Mohamed, S. Lee, Z. Horita, Nanostructure control of age-hardenable Al 2024 alloy by high-pressure torsion, *Mater. Sci. Eng. IOP Journal, NanoSPD6 Proceedings*, 83 (2014) (6p).

- [27] I.F. Mohamed, Y. Yonenaga, S. Lee, K. Edalati, Z. Horita, Age hardening and thermal stability of Al-Cu alloy processed by high-pressure torsion, *Mater. Sci. Eng. A* 627 (2015) 111-118.
- [28] I.F. Mohamed, S. Lee, K. Edalati, Z. Horita, S. Abdullah, M. Z. Omar, W.F.H.W. Zamri, Grain refinement and microstructure evolution in aluminum A2618 alloy by high-pressure torsion, *Jurnal Teknologi* 78: 6-9 (2016) 149-152.
- [29] G.K. Williamson, W.H. Hall, X-ray line broadening from filed aluminium and wolfram, *Acta Mater.* 1 (1953) 22-31.
- [30] A. Vorhauer, R. Pippan, On the homogeneity of deformation by high pressure torsion, *Scr. Mater.* 51 (2004) 921-925.
- [31] K. Edalati, T. Fujioka, Z. Horita, Microstructure and mechanical properties of pure Cu processed by high-pressure torsion, *Mater. Sci. Eng. A* 497 (2008) 168-173.
- [32] K. Edalati, T. Fujioka, Z. Horita, Variation of mechanical properties and microstructures with equivalent strain in pure Fe processed by high-pressure torsion, *Mater. Trans.* 50 (2009) 44-50.
- [33] R.L. Fleischer, Substitutional solution hardening, *Acta Metall.* 11 (1963) 203-209.
- [34] R. Labusch, Statistical theories of solid-solution hardening, *Acta Metall.* 20 (1972) 917-927.
- [35] K. Edalati, D. Akama, A. Nishio, S. Lee, Y. Yonenaga, J.M. Cubero-sesin, Z. Horita, Influence of dislocation-solute atom interactions and stacking fault energy on grain size of single-phase alloys after severe plastic deformation using high-pressure torsion, *Acta Mater.* 69 (2014) 68-77.
- [36] T. Shanmugasundaram, M. Heilmaier, B.S. Murty, V.S. Sarma, On the Hall-Petch relationship in a nanostructured Al-Cu alloy, *Mater. Sci. Eng. A* 527 (2010) 7821-7825.
- [37] J.E. Bailey, P.B. Hirsch, The dislocation distribution, flow stress, and stored energy in cold-worked polycrystalline silver. *Philos. Mag.* 5 (1960) 485-497.
- [38] U.F. Kocks, A.S. Argon, M.F. Ashby, Thermodynamics and kinetics of slip, *Prog. Mater. Sci.* 19 (1975) 1-288.
- [39] N.Q. Chinh, G. Horvath, Z. Horita, T.G. Langdon, A new constitutive relationship for the homogeneous deformation of metals over a wide range of strain, *Acta Mater.* 52 (2004) 3555-3563.
- [40] Y. Chen, N. Gao, G. Sha, S.P. Ringer, M.J. Starink, Microstructural evolution, strengthening and thermal stability of an ultrafine-grained Al-Cu-Mg alloy, *Acta Mater.* 109 (2016) 202-212.

Table 1 Symbols and corresponding physical meaning and values including units for calculations of strengthening components

Symbol	Meaning	Values	Unit
G	Shear modulus	26	GPa
b	Burgers vector magnitude for fcc metal	0.286	nm
ε'_G	Modulus of mismatch	$\varepsilon'_G = 0.59$ for Cu $\varepsilon'_G = -0.41$ for Mg	Dimensionless
ε_b	Atomic size mismatch	$\varepsilon_b = -0.124$ for Cu $\varepsilon_b = 0.105$ for Mg	Dimensionless
m	Mean orientation factor for fcc	3	Dimensionless
φ	Constant	550	Dimensionless
α	Constant	700	Dimensionless
k_y	Hall-Petch coefficient	0.13	MPa/m ^{1/2}
α'	Constant	0.2	Dimensionless

Table 2 Estimated contribution of strengthening components and comparison with experimental data for samples processed by HPT after 5 turns and followed by aging at 423 K for 4 h (all values are in Hv). HV_0 : hardness of coarse-grained pure Al, ΔHV_{SS} : solid solution hardening, ΔHV_{GB} : grain boundary hardening, ΔHV_{Dis} : dislocation hardening, ΔHV_P : precipitation hardening, HV_{Total} : total hardening calculated by Eq. (7), $HV_{Measured}$: measured Vickers hardness.

	Post-HPT Aging time (h)	
	0	4
HV_0	20	20
ΔHV_{SS}	4.5-12.8	4.5-12.8
ΔHV_{GB}	81	78
ΔHV_{Dis}	41	33
ΔHV_P	unknown	95
HV_{Total}	>154	~240
$HV_{Measured}$	253	261

Figure 1 Schematic illustration of HPT disk and locations for hardness measurements, tensile specimen, TEM and XRD disks.

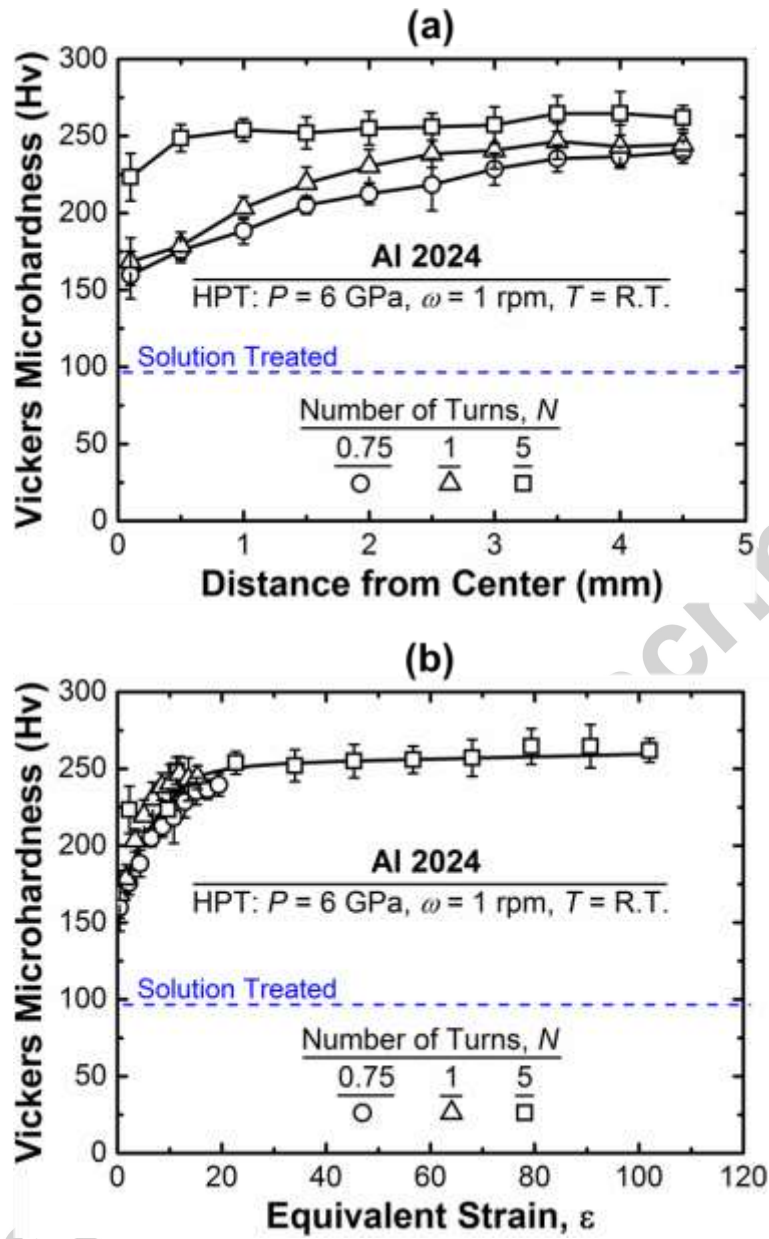


Figure 2 Vickers microhardness plotted against (a) distance from disc center and (b) equivalent strain for samples processed by HPT through 0.75, 1 and 5 turns.

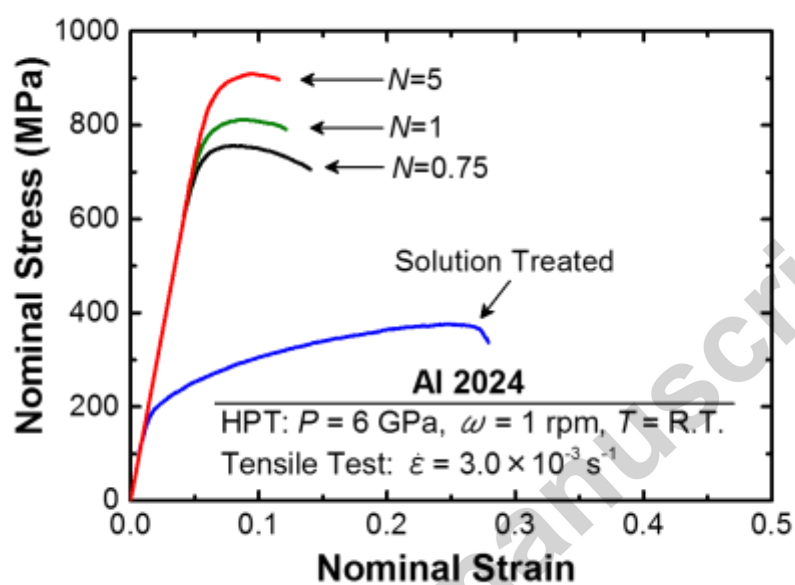


Figure 3 Nominal stress vs nominal strain curves for samples processed by HPT for 0.75, 1 and 5 turns including solution-treated sample.

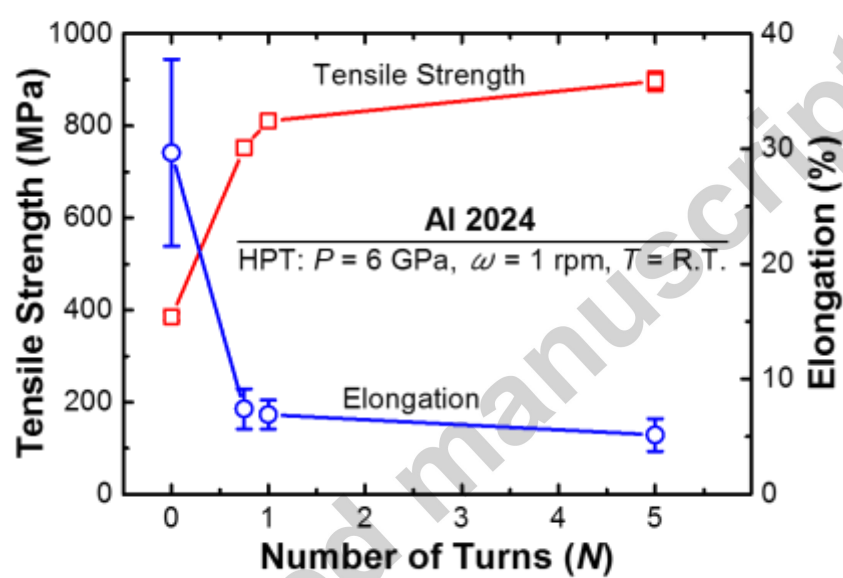


Figure 4 Variation of ultimate tensile strength and total elongation to failure for samples processed by HPT after various turns.

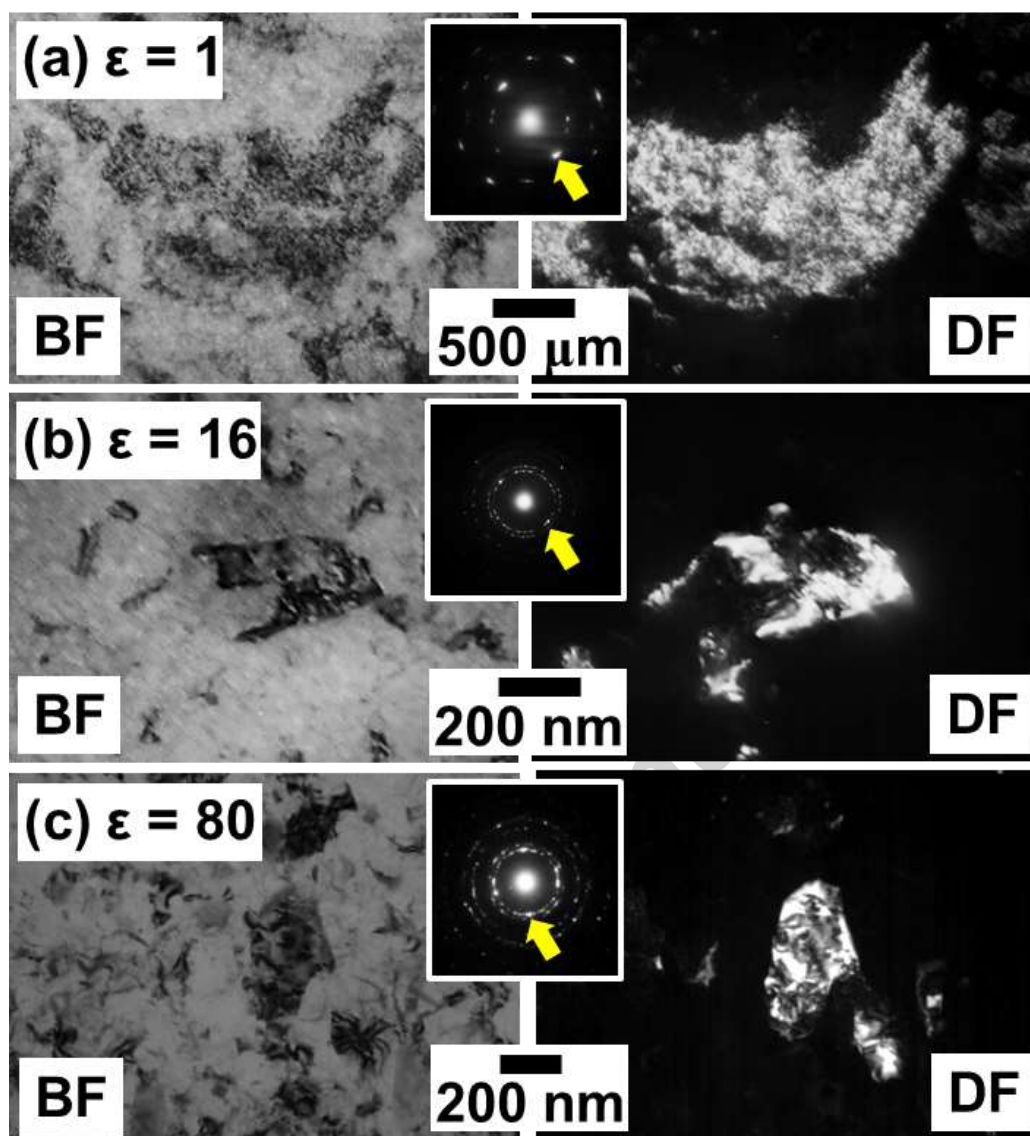


Figure 5 TEM micrographs and SAED patterns after HPT processing at (a) initial stage ($N = 0.75$), (b) middle stage ($N = 1$) and (c) saturated stage ($N = 5$).

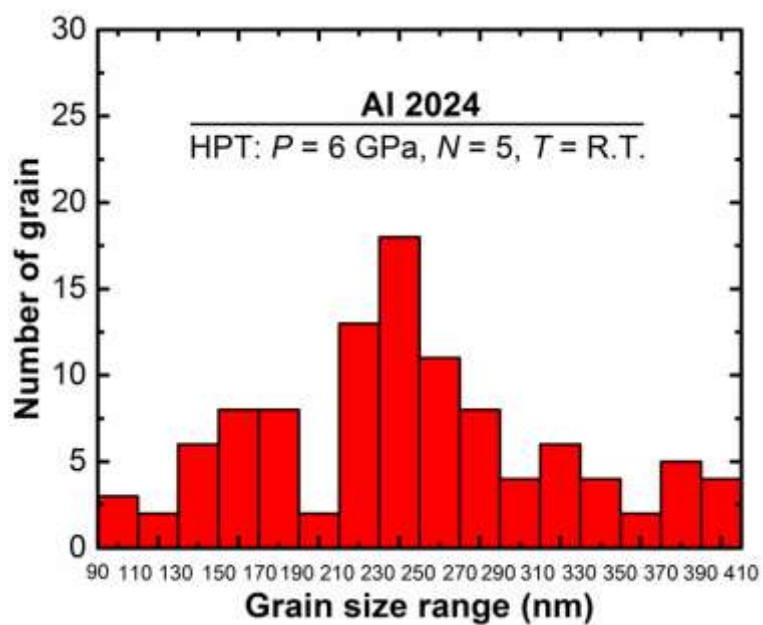


Figure 6 Grain size distribution in HPT processed sample through $N = 5$ turns

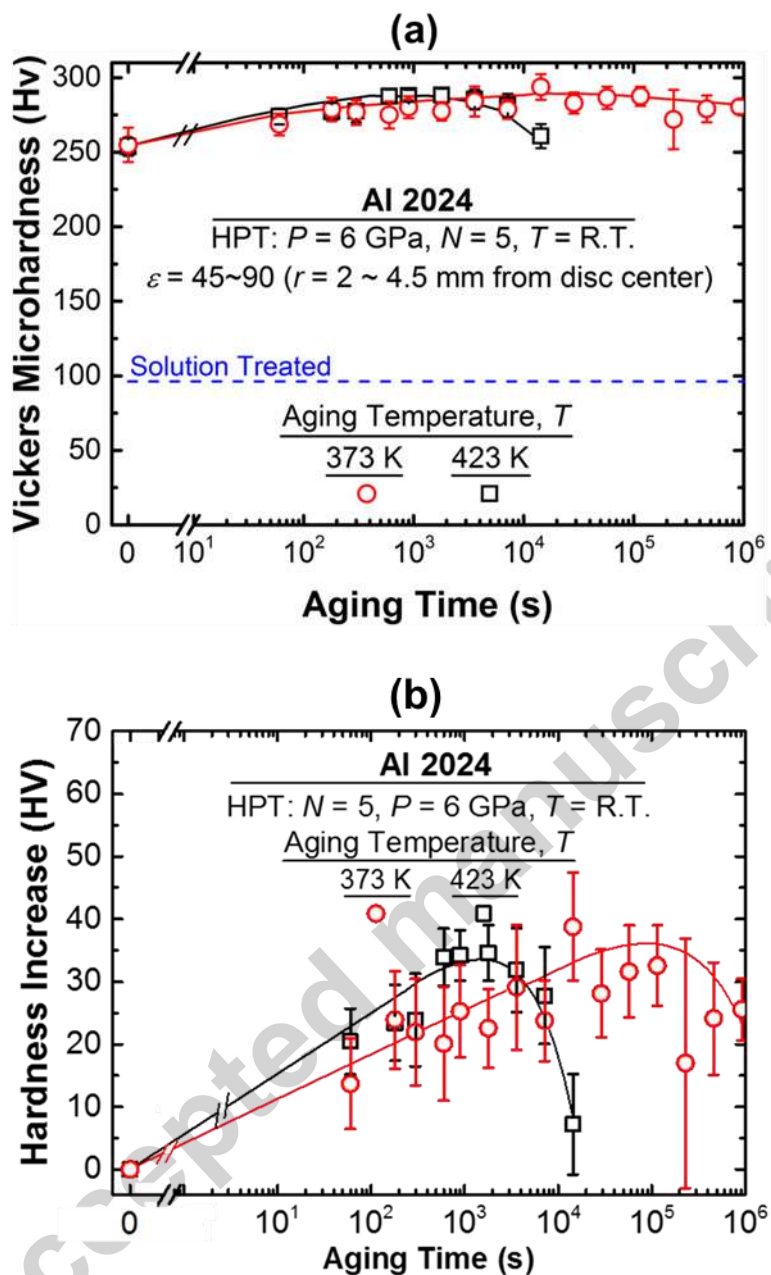


Figure 7 Variations of (a) hardness and (b) hardness increase with aging time for samples processed by HPT through 5 turns. Each hardness value represents average taken from region at saturated hardness level in distance range of 2 - 4.5 mm from disc center ($\varepsilon = 45 \sim 90$).

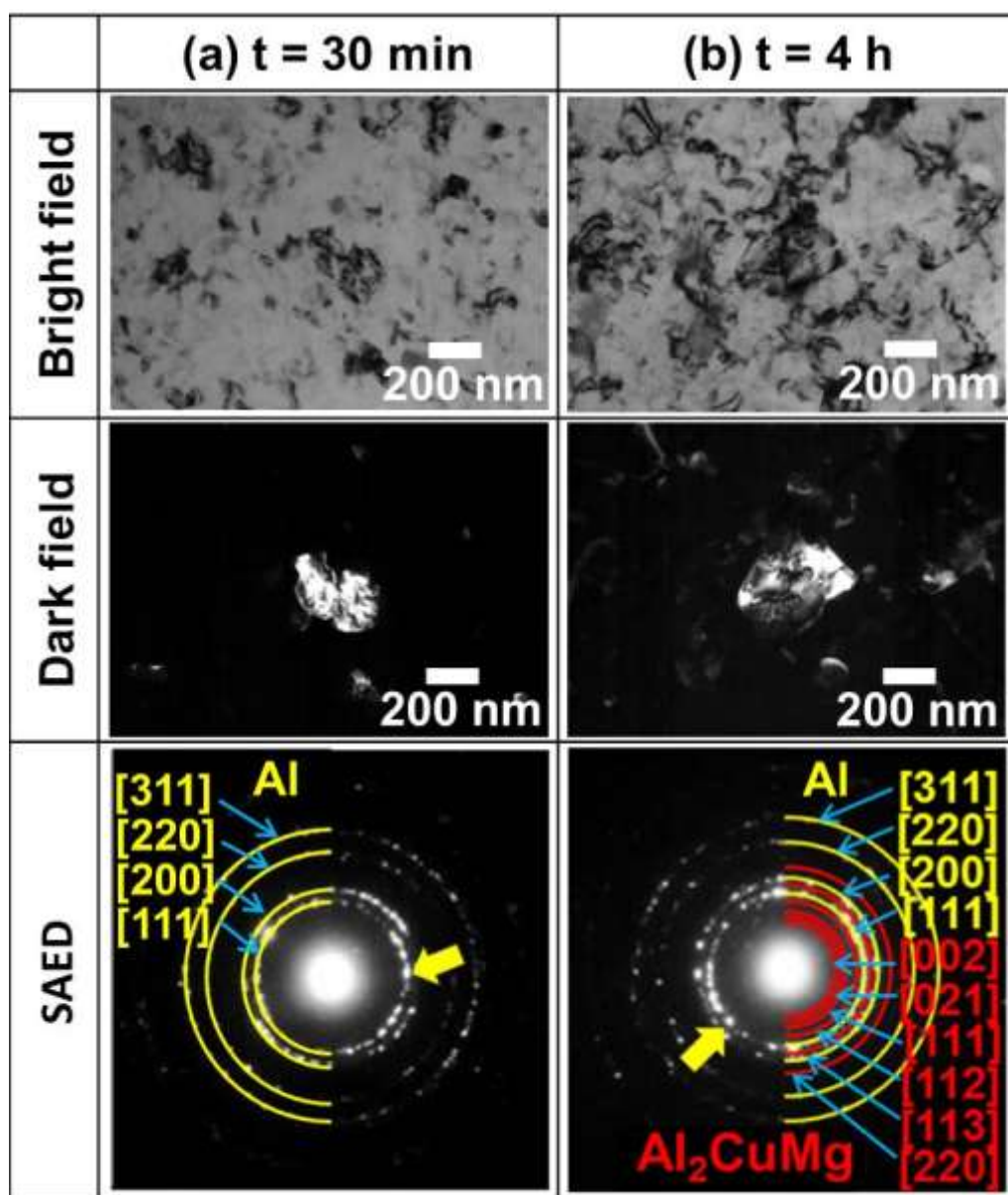


Figure 8 TEM micrographs and SAED patterns of A2024 after HPT processing through $N = 5$ and aging at 423 K for (a) 30 min and (b) 4 h. Arrows indicate diffracted beams for dark-field images. Yellow lines in (a) and (b) shows aluminium matrix while red line in (b) shows S-phase.

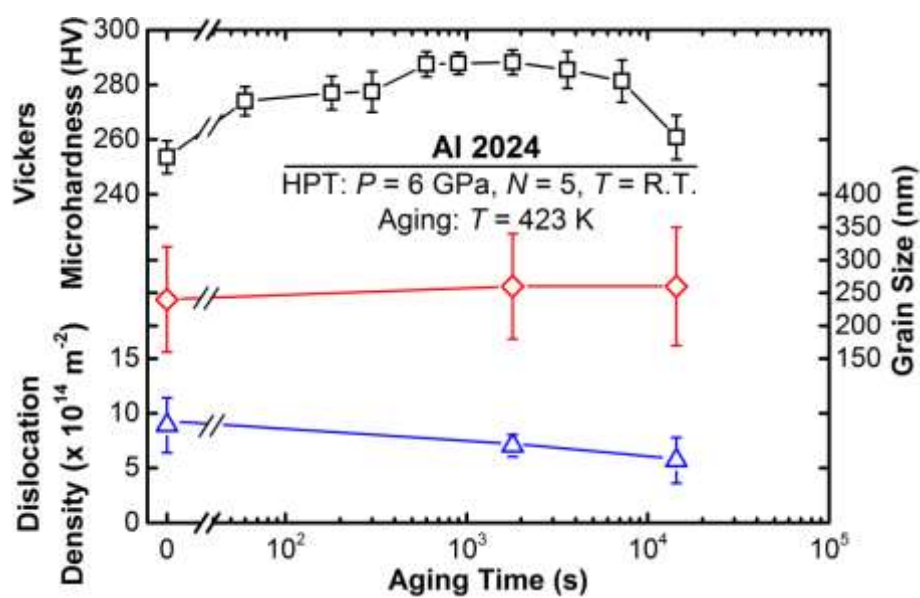


Figure 9 Variation of dislocation density and grain size with aging time for samples processed by HPT through $N=5$ and subsequently aged at 423 K.

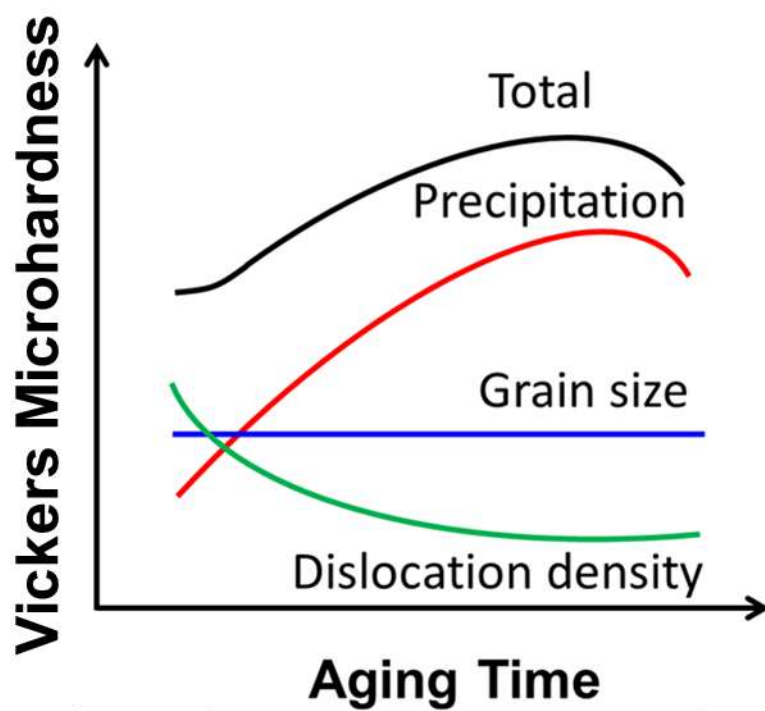


Figure 10 Schematic illustration of strengthening components with aging time.